Journal of
Materials Chemistry C

Accepted Manuscript

This article can be cited before page numbers have been issued, to do this please use: T. Weller, M. Breunig, C. J. Mueller, E. Gann, C. R. McNeill and M. Thelakkat, *J. Mater. Chem. C*, 2017, DOI: 10.1039/C7TC01999H.

ROYAL SOCIETY OF CHEMISTRY

rsc.li/materials-c

View Article Online
DOI: 10.1039/C7TC01999H

Journal Name

ARTICLE

Fluorination in Thieno[3,4-*c*]pyrrole-4,6-idone Copolymers leading to Electron Transport, high Crystallinity and End-on Alignment

Received 00th January 20xx,
Accepted 00th January 20xx

DOI: 10.1039/x0xx00000x

www.rsc.org/

T. Weller,[a] M. Breunig[a], C. J. Mueller[a], E. Gann[c], C. R. McNeill[b] and M. Thelakkat[a*]

A series of copolymers based on thieno[3,4-*c*]pyrrole-4,6-dione and thiophene-phenyl-thiophene with a varying degree of fluorination on the phenyl unit was synthesized by Stille polycondensation. The influence of the degree of fluorination on the optical, thermal and electrochemical properties of these polymers is systematically studied. Additionally, the charge transport in organic field effect transistors (OFETs) as well as the thin film alignment are investigated. After thermal annealing the non-fluorinated as well as difluorinated polymers show ambipolar charge transport in OFETs. In contrast, tetrafluorination results in exclusively n-type behaviour with an electron mobility of 3.7×10^{-4} $cm^2 V^{-1} s^{-1}$. GIWAXS measurements of as-cast and annealed films reveal a very interesting structural alignment in thin films. All polymers show the rarely observed "end-on" orientation, where the polymer chains stand on the substrate. This may be explained by the low molecular weights of these polymers in relation to the film thickness. Fluorination does not influence the microstructural properties, only the propensity of crystallization is increased.

Introduction

In the past, research in the field of polymeric semiconductors has mainly focused on hole-conducting materials synthesized according to the alternating donor-acceptor concept. Recently, there is more interest in electron-conducting materials, also as alternative for fullerene derivatives for applications. In particular naphthalene diimide (NDI) containing copolymers have attracted appreciable attention and have been successfully applied in all-polymer solar cells with efficiencies exceeding 8%.[1] Moreover, it has been repeatedly shown that in all-polymer solar cells, the alignment of polymer chains with their planar π-faces of their backbone, either in an edge-on or face-on manner, considerably affects the device performance.[2,3]

Thieno[3,4-*c*]pyrrole-4,6-dione (TPD) is an interesting electron-deficient building block unit due to its high planarity and easy synthetic accessibility.[4,5] Additionally, copolymers incorporating this acceptor unit show high long-term thermal stability, which is also an important and desirable property for application in optoelectronic devices.[6] In general, the TPD moiety has been incorporated as an electron-withdrawing unit in classical low bandgap copolymers to obtain donor materials[7–10], which achieved efficiencies of over 9% in combination with fullerenes in organic solar cells.[11] Also, some of these materials exhibit very high hole mobilites of up to 1.3 $cm^2 V^{-1} s^{-1}$ in OFET devices.[12] Regarding electron transport, only a few examples have been published to date to the best of our knowledge.[13–16] The highest mobility for unipolar n-type transport was reported for copolymers consisting of TPD and isoindigo resulting in a field-effect mobility of 0.01 $cm^2 V^{-1} s^{-1}$.[14] Marks et al. showed ambipolar charge transport in TPD containing copolymers with thiophene as comonomer, where the n-type field effect mobility even exceeds the corresponding hole mobility.[17] Very recently, TPD containing copolymers were applied as acceptor polymers in polymer/polymer blend solar cells with appreciable performance.[18,19]

As comonomer, we selected thiophene-phenyl-thiophene (TPT), which is a rigid building block leading to highly crystalline materials.[20,21] Intrachain nonbonding interactions such as H-S or H-F can improve the planarity and therefore, the crystallinity and stacking behaviour. This is the case for di- and tetrasubstitution of the phenyl protons with small and strongly electronegative fluorine atoms. Crystal structures of the difluorinated small molecules gave evidence that the structure is locked by H-F interactions[20] contrary to some reports where S-F interactions were claimed.[22] Especially Ratner et al. showed that the contribution of S-F interactions is nearly zero as determined by theoretical calculations.[23] Beside the influence of fluorination on the crystalline structure, it is also a powerful tool to improve electron affinity resulting in higher electron transport and in some cases ambipolar charge transport. In the literature, several reports have been

[a] Applied Functional Polymers, Macromolecular Chemistry I, University of Bayreuth, 95440 Bayreuth, Germany.
[b] Department of Materials Engineering, Monash University, Wellington Road, Clayton VIC, 3800, Australia.
[c] Materials Measurement Laboratory, National Institute of Standards and Technology, 100 Bureau Dr, Gaithersburg, MD 20899, USA.
*Corresponding Author: mukundan.thelakkat@uni-bayreuth.de.

† Electronic Supplementary Information (ESI) available: Synthesis and characterization of all monomers, detailed characterization of polymers including NMR, TGA, Flash DSC, OFET and GIWAXS. See DOI: 10.1039/x0xx00000x

View Article Online
DOI: 10.1039/C7TC01999H

published, which show this concept, mainly based on diketopyrrolopyrrole (DPP)[24–28] and naphthalene diimide (NDI)[29,30] copolymers.

In this contribution, we report a series of TPD containing copolymers with different degrees of fluorination of the TPT unit. The synthesis and detailed structural characterization of the copolymers containing TPD and different TPT units are described. To guarantee sufficient solubility, the TPD unit was decorated with a branched octyldodecyl substituent. The comonomer TPT was di- and tetrafluorinated (TPF_2T and TPF_4T) in order to gradually increase the degree of fluorination. The systematic study of the influence of fluorination on the properties regarding structure formation and OFET mobilities are given here. Especially, we were interested to elucidate the influence of fluorination on crystallinity and consequently on charge transport. Very surprisingly, the GIWAXS studies show end-on alignment of polymer chains, which is usually rare in the case of conjugated polymers without any reactive grafting of the chain to a substrate.

Experimental Part

Materials and Methods

All commercially available reagents were used as received unless otherwise noted. Reactions under microwave irradiation were conducted in a Biotage Initiator Eight+ Microwave. Size exclusion chromatography (SEC) was carried out on an Agilent (Polymer Laboratories Ltd.) PL-SEC 220 high temperature chromatographic unit equipped with three linear mixed bed columns (PSS Polefin linear XL) and DP and RI detectors. Analysis was performed at 160 °C using 1,2,4-trichlorobenzene as the eluent. The samples were prepared by dissolving the polymer (0.1 wt-%) in the solvent in an external oven and the solutions were injected and eluted without filtration. The molecular weights of the samples were referenced to polystyrene standards (M_w = 518-2,600,000 g mol^{-1}, K = 12.100 and Alpha = 0.707). Cyclic voltammetric measurements were carried out in thin films under moisture- and oxygen-free conditions using a three-electrode assembly connected to a potentiostat (model 263A, EG&G Princeton Applied Research) at a scanning rate of 100 m V s^{-1}. As electrolyte solution tetra-*n*-butylammonium hexafluorophosphate in acetonitrile with a concentration of 0.1 M was used. Glass substrates coated with ITO (10 Ω/□) were used as working electrode, on which thin films from $CHCl_3$ solutions with a concentration of 5 mg/mL were spin coated at 1500 rpm. A platinum wire in the respective electrolyte solution and $Ag/AgNO_3$ in acetonitrile (0.1 M) were used as counter and reference electrode, respectively. Each measurement was calibrated by the internal standard ferrocene/ferrocenium. UV/Vis spectra were recorded on a JASCO V-670 spectrophotometer. Fluorescence spectroscopy was performed on a JASCO FP-8600 spectrofluorometer using the wavelength maximum of transition for absorption as excitation wavelength. The optical properties were analysed either in chloroform solutions (0.01 mg/mL) using quartz cuvettes with an internal diameter of 10 mm or in thin films spin coated on glass slides from chloroform solutions (5 mg/mL) at 1500 rpm. For thermogravimetric analysis (TGA) a Netzsch STA 449 F3 Jupiter was used at a scanning rate of 10 K min^{-1} under nitrogen atmosphere. The temperature of decomposition, $T_{5\%}$ was determined at 5% mass loss. Flash DSC measurements were conducted on a Mettler-Toledo Flash DSC 1 at scanning rates between 50 and 1000 K min^{-1} under nitrogen. The organic thin film transistor substrates with a bottom gate, bottom contact architecture were purchased form Fraunhofer IPMS (OFET Gen. 4). As substrate and gate electrode a heavily n-doped silicon wafer (doping at wafer surface: n ~ 3 x 10^{17} cm^{-3}) was used. The gate electrode is separated from the source and drain electrodes by thermal silicon dioxide (Standard 90/230 nm) as dielectric. Source and drain electrodes are made from gold with a thickness of 30 nm adhered to the dielectric by a layer of 10 nm ITO. One chip carries four groups with four identical transistors with a channel length of 2.5, 5, 10 and 20 µm, respectively, and a channel width of 10 mm. The substrates were rinsed with acetone and purified by ultasonification in acetone and 2-propanol for 10 min each. After plasma treatment for 15 min at 50 °C, silanisation with octadecyltrichlorosilane in toluene (1 vol%) at 60 °C for 1 h was conducted. The devices were rinsed with toluene and stored in 2-propanol until spin coating. Films were spin coated from chloroform solutions (10 mg/mL) at 5000 rpm under ambient conditions and directly transferred into the glove box. Current-voltage characteristics were measured under nitrogen atmosphere using an Agilent B1500 Semiconductor Parameter Analyzer. Annealing was performed at 250 °C for 15 min under nitrogen atmosphere. The charge carrier mobility was calculated using equation (1), where I_{DS} is the drain-source current, V_G the gate voltage, L the channel length, W the channel width and C_i the capacitance. Therefore, the square root of the drain-source current $I_{DS}^{1/2}$ was plotted against the gate voltage V_G in the saturation regime and the slope of the resulting curve was determined to calculate the mobility.

$$\mu_{sat} = \left(\frac{\partial\sqrt{I_{DS}}}{\partial V_G}\right)^2 \cdot \frac{2L}{WC_i} \qquad (1)$$

Synthesis procedures

General procedure for the Stille polycondensation: A microwave vial was loaded with the monomers 1,3-dibromo-5-(2-octyldodecyl)-4*H*-thieno[3,4-*c*]pyrrol-4,6(5*H*)-dione **1** (1 eq) and the different TPTs **2** (1 eq) and tri(*o*-tolyl)phosphine (0.12 eq) and chlorobenzene (77 mM) was added. After degassing by argon bubbling for 10 min, tris(dibenzylideneacetone)di-palladium(0) (0.03 eq) was added. The microwave vial was sealed and purged with argon once more. The polymerization reaction was conducted at 180 °C for 1 h under microwave irradiation. After cooling to room temperature, 2-tributyltinthiophene was added to end-cap the polymers and the reaction mixture was stirred for 5 min at 180 °C. The end-capping step was, subsequently, repeated with 2-

View Article Online
DOI: 10.1039/C7TC01999H

bromothiophene for 10 min. The polymer solution was precipitated in methanol (300 mL) and filtered. Further purification was carried out by sequential Soxhlet extraction using methanol, acetone and hexane. Finally, the polymer was collected by chloroform extraction and the solution was concentrated under reduced pressure. Precipitation in methanol, filtration and drying in vacuum yielded the desired polymer.

P(TPD-TPT): Following the general procedure, a solution of 1,3-dibromo-5-(2-octyldodecyl)-4*H*-thieno[3,4-*c*]pyrrol-4,6(5*H*)-dione **1** (183 mg, 0.309 mmol, 1 eq), 1,4-bis(5-(trimethyl-stannyl)thiophen-2-yl)benzene (176 mg, 0.309 mmol, 1 eq) **2a**, tri(*o*-tolyl)phosphine (11.3 mg, 0.037 mmol, 0.12 eq) and tris(dibenzylideneacetone)dipalladium(0) (8.50 mg, 9.27 µmol, 0.03 eq) in 4 mL chlorobenzene was stirred for 1 h at 180 °C yielding P(TPD-TPT) (120 mg, 55%) as a black solid. ^{1}H NMR (300 MHz, $CDCl_3$): δ = 5.06-8.28 (8H), 2.90-3.88 (2H), 0.31-2.16 (39H) ppm.

P(TPD-TPF$_2$T): Following the general procedure, a solution of 1,3-dibromo-5-(2-octyldodecyl)-4*H*-thieno[3,4-*c*]pyrrol-4,6(5*H*)-dione **1** (183 mg, 0.309 mmol, 1 eq), (5,5'-(2,5-difluoro-1,4-phenylene)bis(thiophene-5,2-diyl))bis(trimethyl-stannane) **2b** (187 mg, 0.309 mmol, 1 eq), tri(*o*-tolyl)phosphine (11.3 mg, 0.037 mmol, 0.12 eq) and tris(dibenzylidene-acetone)dipalladium(0) (8.50 mg, 9.27 µmol, 0.03 eq) in 4 mL chlorobenzene was stirred for 1 h at 180 °C yielding P(TPD-TPF$_2$T) (100 mg, 44%) as a black solid. ^{1}H NMR (300 MHz, $CDCl_3$): δ = 5.06-8.63 (6H), 2.90-3.94 (2H), 0.50-2.37 (39H) ppm. ^{19}F NMR (300 MHz, $CDCl_3$): δ = -(114-120) ppm.

P(TPD-TPF$_4$T): Following the general procedure, a solution of 1,3-dibromo-5-(2-octyldodecyl)-4*H*-thieno[3,4-*c*]pyrrol-4,6 (5*H*)-dione **1** (139 mg, 0.234 mmol, 1 eq), (5,5'-(perfluoro-1,4-phenylene)bis(thiophene-5,2-diyl))bis(trimethylstannane) **2c** (150 mg, 0.234 mmol, 1 eq), tri(*o*-tolyl)phosphine (8.57 mg, 0.028 mmol, 0.12 eq) and tris(dibenzylideneacetone) dipalladium(0) (6.45 mg, 7.03 µmol, 0.03 eq) in 3 mL chlorobenzene was stirred for 1 h at 180 °C yielding P(TPD-TPF$_4$T) (145 mg, 80%) as a black solid. ^{1}H NMR (300 MHz, $CDCl_3$): δ = 5.10-8.29 (4H), 2.93-3.96 (2H), 0.53-2.44 (39H) ppm. ^{19}F NMR (300 MHz, $CDCl_3$): δ = -(135-142) ppm.

Results and discussion

Synthesis

The dibromo TPD monomer carrying octyldodecyl solubilizing side chains was synthesized following procedures described in the literature.[31] These long, asymmetric branched side chains were chosen to maintain solubility of the polymer due to the less soluble TPT comonomer. Detailed synthesis procedures of all monomers can be found in the Supporting Information. The syntheses of the stannylated TPT comonomers have already been reported by our group.[27] The dibrominated phenyl derivatives are coupled with thiophene in a Stille reaction followed by bromination and stannylation. For the stannylated TPF$_4$T monomer with tetrafluorinated phenyl unit, we chose an alternative synthetic procedure. The tetrafluorinated phenyl group was flanked with thiophene by direct heteroarylation starting from the corresponding brominated compound as reported in the literature.[32] With palladium acetate as catalyst and potassium pivalate as base in dimethylacetamide, the precursor TPF$_4$T was synthesized in 47% yield. Direct arylation is a powerful tool to combine aromatic units without the need of additional functionalization of one of the coupling compounds with, for example, boronic acid ester or tin compounds. This compound was directly stannylated using *n*-butyl lithium and trimethyltin chloride without prior bromination achieving the stannylated monomer in high purity following a literature described procedure.[33]

Stille polycondensation was applied to polymerize the TPD monomer with the three different TPT monomers carrying different numbers of fluorine atoms. The polymerization was conducted with tris(dibenzylideneacetone)dipalladium(0) as catalyst, tri(*o*-tolylphosphine) as ligand in chlorobenzene for one hour at 180 °C under microwave irradiation. After polymerization, the polymer chains were end-capped using thiophene and were purified by Soxhlet extraction. All the three polymers are well soluble in common organic solvents such as chloroform and toluene. Size exclusion chromatography was conducted in trichlorobenzene at 160 °C due to the strong aggregation of polymer chains at room temperature, especially with increasing degree of fluorination (Fig. 1). The molecular weights (PS calibration) as well as the dispersities are summarized in Table 1. In general, the relative molecular weights obtained for semicrystalline polymers with PS calibration need to be cautiously interpreted in terms of the real molecular weights. However, a comparison among the three polymers provides some indications. With the degree of fluorination, the number-average molecular weights (M_n) increase from 7.90 kg mol^{-1} for P(TPD-TPT) to 11.0 kg mol^{-1} for P(TPD-TPF$_2$T) and to 13.6 kg mol^{-1} for P(TPD-TPF$_4$T). These relative molecular weights (from SEC) do not constitute very high molecular weight. However, for a comparison of the influence of structural changes on crystallinity, orientation and charge transport, these are sufficient, since we have eliminated the influence of end-groups by end-capping. The dispersities for all three polymers are in the range of 1.1-1.3. Even after taking into account the fact that the polymers were purified by Soxhlet extraction, these dispersities are very low for polycondensates. Additionally, the polymers were analysed by

View Article Online
DOI: 10.1039/C7TC01999H

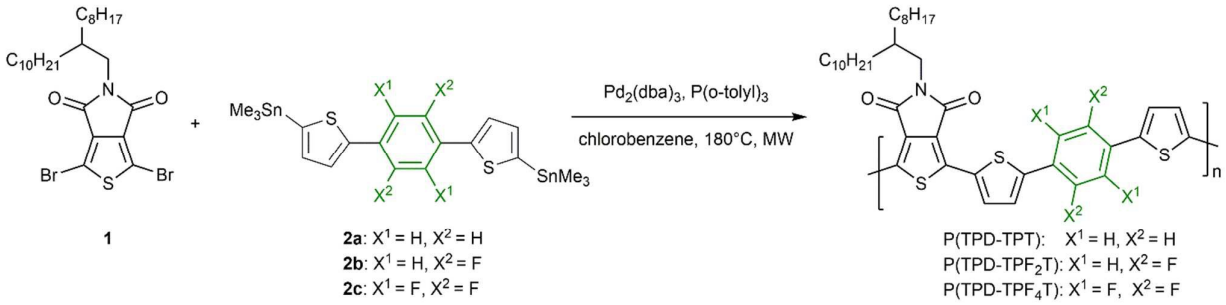

Scheme 1 Synthesis of TPD containing polymers via Stille polymerization in a microwave reactor.

Table 1 SEC, absorption, electrochemical and thermal properties of the TPD containing polymers.

	M_n[a]	M_w[a]	$Đ$	$T_{5\%}$[b]	T_m[c]	T_c[c]	absorbance peaks [nm][d]		E_{opt}[e]	IP[f]	EA[f]
	[kg/mol]	[kg/mol]		[°C]	[°C]	[°C]	solution	film	[eV]	[eV]	[eV]
P(TPD-TPT)	7.85	8.87	1.13	441	400	364	452	475	1.97	-5.46	-3.56
P(TPD-TPF$_2$T)	12.5	12.5	1.14	435	417	394	435	460	1.92	-5.75	-3.64
P(TPD-TPF$_4$T)	13.6	17.6	1.28	442	420	393	427	453	1.95	-6.03	-3.90

[a] Determined by SEC in 1,2,4-trichlorobenzene at 160 °C using PS calibration; [b] decomposition at 5% mass loss determined by TGA at 10 K/min under N_2; [c] melt and crystallization temperature from Flash DSC measurements at 1000 K/min under N_2; [d] maximum absorption peaks from $CHCl_3$ solution and in thin film; [e] optical gap determined by absorption edge in thin films; [f] ionisation potential (IP) and electron affinity (EA) determined form cyclic voltammetry in thin films.

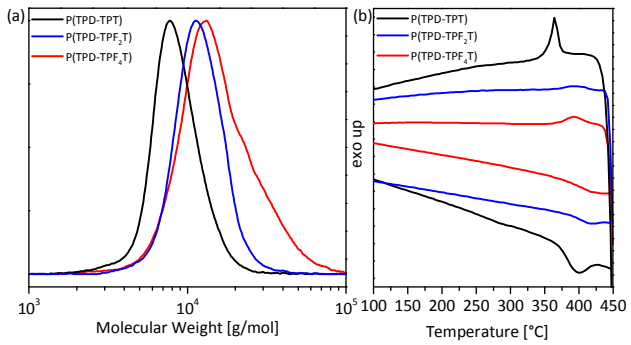

Fig. 1 (a) SEC measurements in trichlorobenzene at 160 °C calibrated with PS standards. (b) Flash DSC traces with a scanning rate of 1000 K/min.

^{1}H- and ^{19}F-NMR and the spectra are depicted in the Supporting Information. In the ^{19}F-NMR spectra, the peaks arising from the fluorine can be assigned. All the three polymers show high thermal stability as shown in TGA measurements. The decomposition temperatures at 5% mass loss are in the range of 435 to 442 °C (Table 1). The crystallization behaviour was investigated with Flash DSC measurements, where the melting and crystallization near the decomposition can be studied due to high scanning rates in the range from 50 to 1000 K/min. In Fig. 1b, the region of interest is shown for a scanning rate of 1000 K/min and the corresponding melting and crystallization temperatures are summarized in Table 1. The complete spectra with all scanning rates are shown in the Supporting Information (see Fig. S2, ESI†). The polymer P(TPD-TPT) shows a clear melting as well as a recrystallization peak at 400 °C and 364 °C, respectively. For the fluorinated polymers, melting and recrystallization are not so pronounced as is the case for the non-fluorinated sample. Due to the fluorination, the adhesion of the polymers to the sample chip in Flash DCS is reduced making the exact thermal measurement difficult. The melting and crystallization temperatures for the di- and tetra-fluorinated polymers are very similar and in the range of 420 °C and 390 °C, respectively. By fluorination, the melting as well as the crystallization temperature is shifted to higher values due to the stronger intermolecular interactions in fluorinated polymers. However, the degree of fluorination does not influence the melting and crystallization temperatures.

Optical properties

In order to study the influence of fluorination on the optical properties, UV/Vis as well as fluorescence measurements were performed in solution and in the solid state. The spectra are shown in Fig. 2 and the absorption peaks in solution and thin films as well as the optical gap obtained from the absorption edge of thin film spectra are summarized in Table 1. In solution, all the three polymers feature a single broad absorption band, which is slightly blue shifted upon fluorination due to the electron-withdrawing properties of the fluorine atoms. Besides this broad absorption band centered at around 420-450 nm, a shoulder at around 550 nm is visible, which arises from an aggregated character of chains in solution. In the solid state, the absorption is red-shifted as compared to their solution spectra due to aggregation; the corresponding spectra can be found in the Supporting Information (see Fig. S3, ESI†). Additionally, the shoulder of aggregated species becomes more prominent. The optical gap was calculated from the absorption edge in thin films resulting in similar values of just below 2 eV for all polymers. In conclusion, fluorination has almost no effect on the optical gap. Excitation at the absorption maximum results in three emission peaks in solution. The intensity of the photoluminescence decreases possibly caused by the stronger aggregation of the fluorine containing polymers in solution.

View Article Online
DOI: 10.1039/C7TC01999H

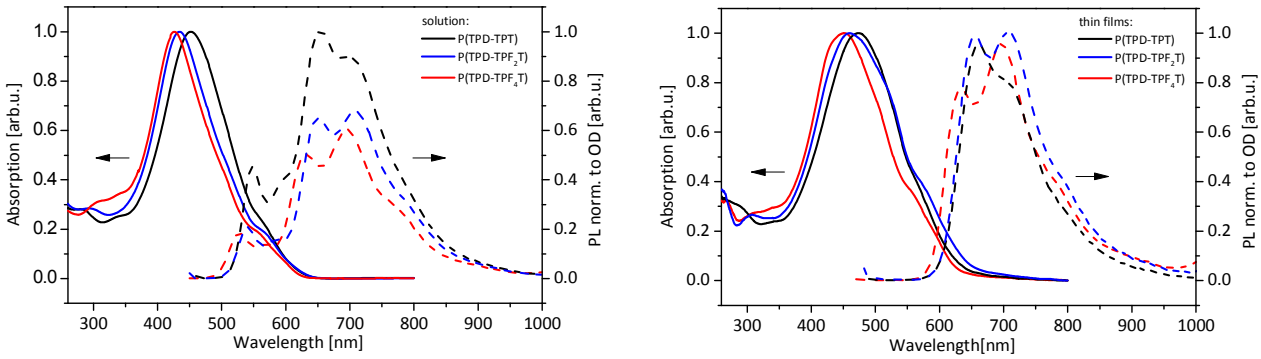

Fig. 2 Comparison of absorption and fluorescence measurements of the three TPD containing polymers in (a) $CHCl_3$ solution and (b) thin films.

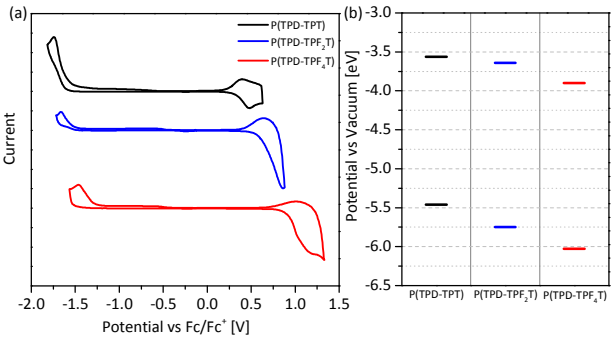

Fig. 3 (a) Cyclic voltammetry measurements in thin films and (b) energy levels calculated from the onset of oxidation and reduction potential.

Moreover, the relative intensities of the vibronic peaks change drastically upon fluorination, which gives a measure for the quality and nature of aggregates.[34] In comparison, the photoluminescence in thin films shift to red and show only the two main emission peaks, whereas the third one becomes weak.

Electrochemical properties

As fluorination is known to have a significant effect on the energy levels of conjugated polymers, the electrochemical properties of thin films of the polymers were analysed by cyclic voltammetry measurements. A three-electrode setup with ITO as working electrode in acetonitrile was used. The cyclic voltammograms are shown in Fig. 3a. A reversible oxidation peak is observed for all the three polymers. Upon fluorination, the oxidation waves are shifted to higher voltages and therefore, the polymers become less oxidizable due to the decreased electron density along the polymer backbone. Additionally, the reduction potential is affected by fluorination and is shifted to lower voltages. In comparison to the oxidation, the reduction seems to be irreversible under our conditions of measurement. The ionization potentials and electron affinities were calculated from the onsets of the reduction and oxidation waves, respectively. These values are only an approximate estimate of the energy levels of thin films in polar solvents and should not be considered as absolute values. In Table 1 the results are summarized and the energy levels are graphically illustrated in Fig. 3b. Difluorination results in a lowering of the IP by 0.3 eV, whereas the EA is almost not affected. By tetrafluorination the IP and EA are further lowered by 0.3 eV, respectively. The lowering of energy levels upon fluorination agrees with similar studies reported in the literature for other low band-gap polymers.[28,35,36] The band-gap determined by cyclic voltammetry is increased by fluorination and remains constant for di- and tetra-fluorinated polymers while both energy levels are lowered. Cyclic voltammetry measurements clearly show that the fluorination has a strong impact on the energy levels, which are gradually lowered upon fluorination.

OFET

The charge carrier mobilities of the polymers were measured using OFETs with a bottom gate, bottom contact architecture. Here, the charge transport occurs in the plane of the thin film at the dielectric interface. Procedures for the device preparation as well as the mobility determination can be found in the experimental section. Measurements were performed on both as-cast films and films annealed at 250 °C for 15 min under nitrogen. In Table 2, the average values for hole and electron mobilities of a minimum of six devices are summarized. The output and transfer characteristics of as-cast and annealed P(TPD-TPT) films are depicted in Fig. 4. In the case of the as-cast film, exclusively p-channel behaviour (Fig. 4a) is observed, whereas the material shows ambipolar character after annealing (Fig. 4b). The hole mobility reaches a value of 1.1 x 10^{-4} $cm^2 V^{-1} s^{-1}$ and the electron mobility 3.4 x 10^{-4} $cm^2 V^{-1} s^{-1}$. Herein, the hole mobility is improved by one order of magnitude after annealing. Interestingly, the polarity of the charge carriers is ambipolar even without fluorination. The same observation was made for the difluorinated polymer P(TPD-TPF_2T) but having slightly higher hole and electron mobilities. The corresponding characteristics can be found in the Supporting Information. No clear transistor behaviour was observed for the tetrafluorinated polymer in the as-cast state. After annealing, exclusively n-channel behaviour (Fig. 4c) was observed with an electron mobility of 3.7 x 10^{-4} $cm^2 V^{-1} s^{-1}$, which is in the same range as the difluorinated polymer. The observed high threshold voltage (see Table S1 in the ESI†) can be ascribed to electron trapping at the dielectric/polymer interface. These measurements give a good insight into the

View Article Online
DOI: 10.1039/C7TC01999H

nature of charge carrier polarity but can be of course shifted to higher values by extensive device optimisation, which is not the main question of this work. After annealing the non-fluorinated as well as the difluorinated polymer shows ambipolar character, whereas by fluorination the hole as well as the electron mobility is increased. In contrast, tetrafluorination generates exclusively n-type behaviour with comparable electron mobilites as for the diflourinated polymers.

Structural analysis - GIWAXS

In order to understand the influence of structural order and alignment in this series of copolymers, grazing incidence wide-angle X-ray scattering (GIWAXS) was performed at the SAXS/WAXS beamline at the Australian Synchrotron.[37] 11 keV electrons were used with scattering patterns recorded on a Dectris Pilatus 1M detector, following procedures detailed elsewhere.[38] Fig. 5 presents the two-dimensional scattering patterns taken of as-cast and annealed films. The images presented in Fig. 5 were taken close to the critical angle (~ 0.12°) which was identified as the angle of incidence that

Table 2 OFET hole and electron mobilites for as-cast films and after thermal annealing at 250 °C for 15 min under nitrogen.

	as-cast	annealed	
	μ_h [a]	μ_h [a]	μ_e [a]
	[$cm^2V^{-1}s^{-1}$]	[$cm^2V^{-1}s^{-1}$]	[$cm^2V^{-1}s^{-1}$]
P(TPD-TPT)	$(2.5 \pm 0.8) \times 10^{-5}$	$(0.4 \pm 0.1) \times 10^{-4}$	$(1.1 \pm 0.1) \times 10^{-4}$
P(TPD-TPF$_2$T)	$(5.0 \pm 1.9) \times 10^{-5}$	$(1.1 \pm 0.5) \times 10^{-4}$	$(3.4 \pm 1.5) \times 10^{-4}$
P(TPD-TPF$_4$T)	-	-	$(3.7 \pm 1.6) \times 10^{-4}$

[a]Hole (μ_h) and electron (μ_e) mobilites calculated from saturation regime. All values are averaged for a minimum of six devices.

View Article Online
DOI: 10.1039/C7TC01999H

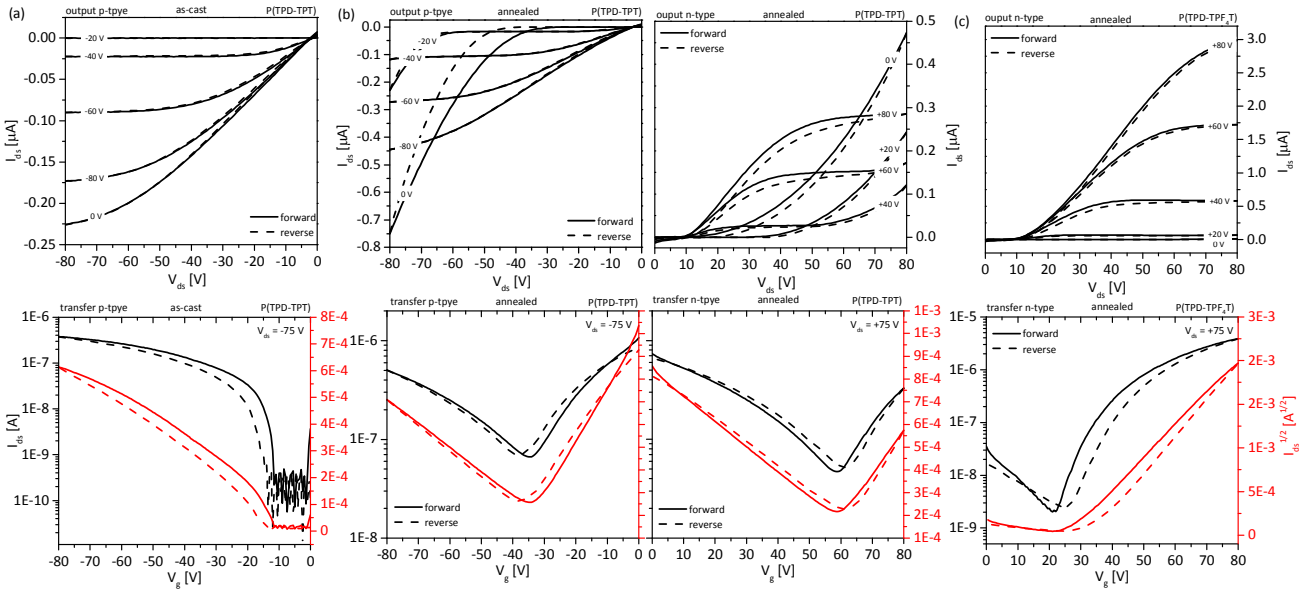

Fig. 4 Representative OFET output (top) and transfer (bottom) characteristics. Solid lines represent forward scans and dashed line reversed scans. (a) p-channel operation of P(TPD-TPT) as-cast and (b) p- and n-channel operation of P(TPD-TPT) after annealing at 250 °C. (c) n-channel operation of P(TPD-TPF$_4$T) after annealing at 250 °C.

gave the maximum scattering intensity. One-dimensional in-plane and out-of-plane scattering profiles are also provided in Fig. 6. All polymers exhibit multiple orders of alkyl stacking, indexed as (k00), even in as-cast films indicating a high propensity of these polymers to crystallise. The alkyl stacking scattering intensity is mainly observed along Q_z for the polymers indicating a predominantly "edge-on" stacking of crystallites. Prominent π-stacking peaks, indexed as (010), are observed in-plane consistent with this molecular orientation. Alkyl stacking scattering intensity is also observed from crystallites at other azimuthal angles indicating the presence of crystallites with orientation other than edge-on. A backbone stacking peak, indexed as (001), is also seen at a Q value of ~ 3.2 nm^{-1}. Curiously this backbone stacking peak is observed out-of-plane (along Q_z, just below the second order alkyl stacking peak) as well as along Q_{xy}. Generally, for conjugated polymers the backbone is thought to lie flat in the plane of the film which is likely to be the case for thin films where the film thickness is smaller than the contour length of the polymer. Here, however, a significant (001) peak intensity is observed out-of-plane indicating the "end-on" orientation of some polymer chains. This unusual observation is thought to be due to the relatively low molecular weight of these polymers and the relatively large film thickness of these films (around 120 nm) relative to the contour length. The series of alkyl stacking peaks along Q_z and the presence of a backbone stacking peak along Q_z indicates separate populations of polymer chains with distinct orientation. The lamellar stacking peak associated with end-on oriented chains is expected to be found along Q_{xy} suggesting that the in-plane (100) peak is associated with end-on oriented chains rather than face-on oriented crystallites. Such an assignment is consistent with the fact that only a very weak π-stacking peak is observed out-of-plane. For both edge-on and end-on oriented chains the π-stacking peak is expected to be found along Q_{xy}.

Despite having different degrees of fluorination, the polymers all possess similar crystallographic parameters (see Fig. S8 in the ESI†). A π-π stacking distance of 0.38 ± 0.01 nm is observed for all polymers with there being more variation with annealing than from polymer to polymer (the effect of annealing of the π-π stacking however is not systematic). Fluorination does seem to lead to a tighter alkyl stacking distance, decreasing from 3.4 nm to 3.3 nm going from P(TPD-TPT) to P(TPD-TPF$_4$T), although a slight increase is observed for P(TPD-TPF$_2$T) (~ 3.45 nm). Judging by the increase in scattering intensity of the alkyl stacking peaks, there appears to be an increase in the degree of crystallinity with fluorination, particularly in the as-cast films. This would suggest that while fluorination has not affected the molecular packing of the polymers, it has increased the propensity of chains to crystallise during solution deposition.

Relating the microstructural data to the OFET data, the similar charge carrier mobilities achieved for the different polymers can be seen as being consistent with the similar microstructural

View Article Online
DOI: 10.1039/C7TC01999H

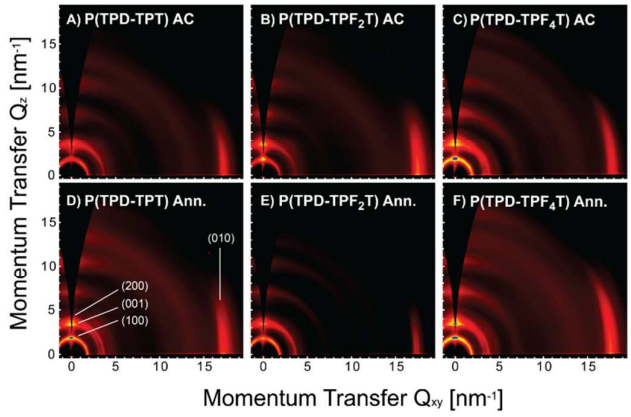

Fig. 5 Two-dimensional GIWAXS patterns of P(TPD-TPT) (a, d) P(TPD-TPF$_2$T) (b, e) and P(TPD-TPF$_4$T) (c, f). (a-c) show as-cast films while (d-f) show films annealed at 250 °C.

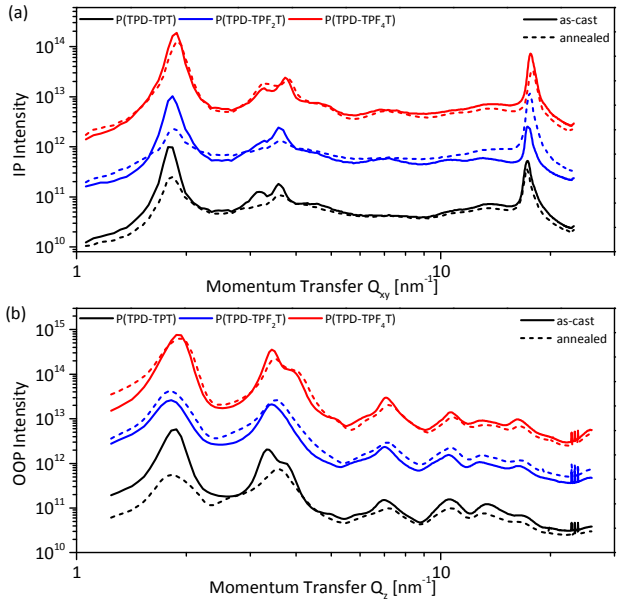

Fig. 6 One-dimensional GIWAXS scattering profiles of P(TPD-TPT), P(TPD-TPF$_2$T) and P(TPD-TPF$_4$T) taken along the in-plane (a) and out-of-plane (b) directions.

properties. The fact that hole conduction was not observed in the case of P(TPD-TPF$_4$T) is then likely due to difficulties in injecting holes into the deep HOMO of this polymer.

Conclusions

We have demonstrated that fluorination is a powerful tool to generate exclusively n-type behaviour in thieno[3,4-*c*]pyrrole-4,6-dione based polymers. For this, thieno[3,4-*c*]pyrrole-4,6-dione was successfully copolymerized with thiophene-phenyl-thiophene moieties with different degrees of fluorination. Whereas the optical properties are almost not affected by fluorination, the energy levels, both IP and EA, are lowered. In GIWAXS measurements the thin film alignment of these polymers surprisingly show end-on alignment, which is rarely observed in conjugated polymers without any reactive grafting of the chains to the substrate. This may be explained by the relatively low molecular weights and therefore, small contour length of these polymer in comparison to the film thickness.

Acknowledgements

We acknowledge finance support from Bavarian State Ministry for Education, Science and the Arts under the SolTech project. T.W. thanks the Elite Network Bavaria Macromolecular Science programme at the University of Bayreuth. This research was undertaken in part on the SAXS/WAXS beamline at the Australian Synchrotron, Victoria, Australia. C.R.M. acknowledges support from the Australian Research Council (DP130102616).

References

1. L. Gao, Z.-G. Zhang, L. Xue, J. Min, J. Zhang, Z. Wei and Y. Li, *Adv. Mater.*, 2016, **28**(9), 1884.
2. J. W. Jo, J. W. Jung, H. Ahn, M. J. Ko, A. K.-Y. Jen and H. J. Son, *Adv. Energy Mater.*, 2017, **7**(1), 1601365.
3. K. Zhou, R. Zhang, J. Liu, M. Li, X. Yu, R. Xing and Y. Han, *ACS applied materials & interfaces*, 2015, **7**(45), 25352.
4. N. Zhou, X. Guo, R. Ponce Ortiz, T. Harschneck, E. F. Manley, S. J. Lou, P. E. Hartnett, X. Yu, N. E. Horwitz, P. Mayorga Burrezo, T. J. Aldrich, J. T. Lopez Navarrete, M. R. Wasielewski, L. X. Chen, R. P. H. Chang, A. Facchetti and T. J. Marks, *J. Am. Chem. Soc.*, 2015, **137**(39), 12565.
5. J. Warnan, C. Cabanetos, A. El Labban, M. R. Hansen, C. Tassone, M. F. Toney and P. M. Beaujuge, *Adv. Mater.*, 2014, **26**(25), 4357.
6. A. Tournebize, J.-L. Gardette, C. Taviot-Guého, D. Bégué, M. A. Arnaud, C. Dagron-Lartigau, H. Medlej, R. C. Hiorns, S. Beaupré, M. Leclerc and A. Rivaton, *Polym. Degrad. Stab.*, 2015, **112**, 175.
7. M.-C. Yuan, M.-Y. Chiu, S.-P. Liu, C.-M. Chen and K.-H. Wei, *Macromolecules*, 2010, **43**(17), 6936.
8. Z. Li, S.-W. Tsang, X. Du, L. Scoles, G. Robertson, Y. Zhang, F. Toll, Y. Tao, J. Lu and J. Ding, *Adv. Funct. Mater.*, 2011, **21**(17), 3331.
9. Y. Zou, A. Najari, P. Berrouard, S. Beaupré, B. R. Aïch, Y. Tao and M. Leclerc, *Journal of the American Chemical Society*, 2010, **132**(15), 5330.
10. Y. Zhang, S. K. Hau, H.-L. Yip, Y. Sun, O. Acton and A. K.-Y. Jen, *Chem. Mater.*, 2010, **22**(9), 2696.
11. J.-H. Kim, J. B. Park, I. H. Jung, A. C. Grimsdale, S. C. Yoon, H. Yang and D.-H. Hwang, *Energy Environ. Sci.*, 2015, **8**(8), 2352.
12. Q. Wu, M. Wang, X. Qiao, Y. Xiong, Y. Huang, X. Gao and H. Li, *Macromolecules*, 2013, **46**(10), 3887.
13. F. Grenier, P. Berrouard, J.-R. Pouliot, H.-R. Tseng, A. J. Heeger and M. Leclerc, *Polym. Chem.*, 2013, **4**(6), 1836.
14. G. Kim, A.-R. Han, H. R. Lee, J. Lee, J. H. Oh and C. Yang, *Chem. Commun.*, 2014, **50**(17), 2180.

View Article Online
DOI: 10.1039/C7TC01999H

15. W. Wang, S. Yan, W. Lv, Y. Zhao, M. Sun, M. Zhou and Q. Ling, *Journal of Macromolecular Science, Part A*, 2015, **52**(11), 892.
16. Z. A. Wang, J. Kuwabara, A. Ichige, T. Yasuda and T. Kanbara, *Synthetic Metals*, 2016, **222**, 383.
17. X. Guo, R. P. Ortiz, Y. Zheng, M.-G. Kim, S. Zhang, Y. Hu, G. Lu, A. Facchetti and T. J. Marks, *J. Am. Chem. Soc.*, 2011, **133**(34), 13685.
18. S. Liu, Z. Kan, S. Thomas, F. Cruciani, J.-L. Bredas and P. M. Beaujuge, *Angew. Chem., Int. Ed.*, 2016, **55**(42), 12996.
19. S. Liu, X. Song, S. Thomas, Z. Kan, F. Cruciani, F. Laquai, J.-L. Bredas and P. M. Beaujuge, *Adv. Energy Mater.*, 2017, **376**, 1602574.
20. D. J. Crouch, P. J. Skabara, J. E. Lohr, J. J. W. McDouall, M. Heeney, I. McCulloch, D. Sparrowe, M. Shkunov, S. J. Coles, P. N. Horton and M. B. Hursthouse, *Chem. Mater.*, 2005, **17**(26), 6567.
21. D. J. Crouch, P. J. Skabara, M. Heeney, I. McCulloch, S. J. Coles and M. B. Hursthouse, *Chem. Commun.*, 2005(11), 1465.
22. H. G. Kim, B. Kang, H. Ko, J. Lee, J. Shin and K. Cho, *Chem. Mater.*, 2015, **27**(3), 829.
23. N. E. Jackson, B. M. Savoie, K. L. Kohlstedt, M. La Olvera de Cruz, G. C. Schatz, L. X. Chen and M. A. Ratner, *J. Am. Chem. Soc.*, 2013, **135**(28), 10475.
24. P. Sonar, J. Chang, Z. Shi, J. Wu and J. Li, *J. Mater. Chem. C*, 2015, **3**(9), 2080.
25. J. Y. Lee, J. W. Jo and W. H. Jo, *Org. Electron.*, 2015, **20**, 125.
26. C. J. Mueller, C. R. Singh, M. Fried, S. Huettner and M. Thelakkat, *Adv. Funct. Mater.*, 2015, **25**(18), 2725.
27. C. J. Mueller, E. Gann, C. R. McNeill and M. Thelakkat, *J. Mater. Chem. C*, 2015, **3**(34), 8916.
28. J. H. Park, E. H. Jung, J. W. Jung and W. H. Jo, *Advanced materials (Deerfield Beach, Fla.)*, 2013, **25**(18), 2583.
29. X. Li, X. Liu, P. Sun, Y. Feng, H. Shan, X. Wu, J. Xu, C. Huang, Z.-K. Chen and Z.-X. Xu, *RSC Adv*, 2017, **7**(28), 17076.
30. A. Luzio, D. Fazzi, F. Nübling, R. Matsidik, A. Straub, H. Komber, E. Giussani, S. E. Watkins, M. Barbatti, W. Thiel, E. Gann, L. Thomsen, C. R. McNeill, M. Caironi and M. Sommer, *Chem. Mater.*, 2014, **26**(21), 6233.
31. A. Najari, S. Beaupré, P. Berrouard, Y. Zou, J.-R. Pouliot, C. Lepage-Pérusse and M. Leclerc, *Adv. Funct. Mater.*, 2011, **21**(4), 718.
32. R. Matsidik, J. Martin, S. Schmidt, J. Obermayer, F. Lombeck, F. Nubling, H. Komber, D. Fazzi and M. Sommer, *J. Org. Chem.*, 2015, **80**(2), 980.
33. N. J. Findlay, J. Bruckbauer, A. R. Inigo, B. Breig, S. Arumugam, D. J. Wallis, R. W. Martin and P. J. Skabara, *Adv. Mater.*, 2014, **26**(43), 7290.
34. F. C. Spano, J. Clark, C. Silva and R. H. Friend, *The Journal of chemical physics*, 2009, **130**(7), 74904.
35. Z. Li, J. Lu, S.-C. Tse, J. Zhou, X. Du, Y. Tao and J. Ding, *J. Mater. Chem.*, 2011, **21**(9), 3226.
36. K. Kawashima, T. Fukuhara, Y. Suda, Y. Suzuki, T. Koganezawa, H. Yoshida, H. Ohkita, I. Osaka and K. Takimiya, *Journal of the American Chemical Society*, 2016, **138**(32), 10265.
37. N. M. Kirby, S. T. Mudie, A. M. Hawley, D. J. Cookson, H. D. T. Mertens, N. Cowieson and V. Samardzic-Boban, *J Appl Crystallogr*, 2013, **46**(6), 1670.
38. T. T. Do, K. Rundel, Q. Gu, E. Gann, S. Manzhos, K. Feron, J. Bell, C. R. McNeill and P. Sonar, *New J. Chem.*, 2017, **41**(8), 2899.

View Article Online
DOI: 10.1039/C7TC01999H

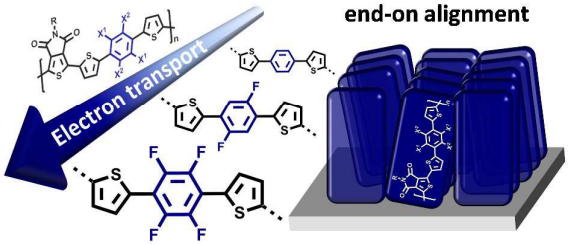

GIWAXS measurements confirm end-on alignment for TPD-copolymers obtained from Stille polycondensation using fluorinated and non-fluorinated comonomers.